Title

The V-motifs facilitate the substrate capturing step of the PTS elevator mechanism

Journal

Journal of Structural Biology, 196(3)

ISSN

1047-8477

Authors

Vastermark, Ake
Driker, Adelle
Weng, Jingwei
et al.

Publication Date

2016-12-01

DOI

10.1016/j.jsb.2016.10.002

Peer reviewed

Journal of Structural Biology 196 (2016) 496–502

Contents lists available at ScienceDirect

Journal of Structural Biology

journal homepage: www.elsevier.com/locate/yjsbi

Technical Note

The V-motifs facilitate the substrate capturing step of the PTS elevator mechanism

Ake Vastermark [a,*], Adelle Driker [a], Jingwei Weng [b], Xiaochun Li [c], Jiawei Wang [d], Milton H. Saier [a]

[a] Department of Molecular Biology, University of California at San Diego, La Jolla, CA 92093-0116, USA
[b] Shanghai Key Laboratory of Molecular Catalysis and Innovative Materials, Department of Chemistry and Institute of Biomedical Sciences, Fudan University, Shanghai, People's Republic of China
[c] Laboratory of Cell Biology, Howard Hughes Medical Institute, The Rockefeller University, New York, NY 10065, USA
[d] State Key Laboratory of Biomembrane and Membrane Biotechnology, School of Life Sciences, Tsinghua University, Beijing, People's Republic of China

ARTICLE INFO

Article history:
Received 5 August 2016
Received in revised form 2 October 2016
Accepted 5 October 2016
Available online 6 October 2016

ABSTRACT

We propose that the alternative crystal forms of outward open UlaA (which are experimental, not simulated, and contain the substrate in the cavity) can be used to interpret/validate the MD results from MalT (the substrate capture step, which involves the mobile second TMSs of the V-motifs, TMSs 2 and 7). Since the crystal contacts are the same between the two alternative crystal forms of outward open UlaA, the striking biological differences noted, including rearranged hydrogen bonds and salt bridge coordination, are not attributable to crystal packing differences. Using transport assays, we identified G58 and G286 as essential for normal vitamin C transport, but the comparison of alternative crystal forms revealed that these residues to unhinge TMS movements from substrate-binding side chains, rendering the mid-TMS regions of homologous TMSs 2 and 7 relatively immobile. While the TMS that is involved in substrate binding in MalT is part of the homologous bundle that holds the two separate halves of the transport assembly (two proteins) together, an unequal effect of the two knockouts was observed for UlaA where both V-motifs are free from such dimer interface interactions.

1. Introduction

Seldom is the same conformational state of a protein crystallized twice in alternative crystal forms, using the same crystallization conditions, in the same lattice, but in two different space groups (UlaA in the outward open state; $P2_1A$ which is more unusual, and C2A which is more frequent). In this article, we propose that this scenario presents valuable information about structural flexibility, similar to the information obtained from temperature factors or from Normal Mode Analysis, yet coming from a different and independent information source. We attempt to subtract the estimates of local instability from the different information sources, to gauge where they agree and disagree. To aid the comparison, we establish a reference point in UlaA by a functional transport assay and confirm it by a superimposition experiment. These reference points are two local and homologous regions of local stability, G58 and G286, and assist in the interpretation of comparative instability data.

What originally prompted our analysis was the fact that two glycines 58 and 286 that cropped up in a functional analysis of UlaA did not appear to be in mobile regions of the UlaA protein based on temperature factor data. This is in contrast to the notion that other well known mid-TMS glycines provide flexibility, such as the mid-TMS glycines of spiny helices of APC transporters (including Gly 25 and 206 of AdiC, PDB: 3L1L) (Västermark and Saier, 2014). While Gly25 and 206 apparently interrupt the helical structure of the substrate channel proximal TMSs, they do not revent measurable flexibility in temperature factor plots. Glycines 58 and 286 of UlaA are, in contrast to such flexible glycines of APC transporters, located near the membrane and not in the protein interior or substrate translocation channel. We wanted to determine using NMA if the apparent lack of flexibility could be an artifact caused by the crystal packing environment and discovered that unlike many proteins, UlaA has two alternative crystal forms in the same conformational state, providing a third source of flexibility information.

Abbreviations: C2A, $P2_1A$, space group names; APC, Amino acid-Polyamine organoCation superfamily of secondary carriers; PTS, bacterial Phospho-Transferase System; NMA, Normal Mode Analysis.

* Corresponding author.
E-mail address: msaier@ucsd.edu (A. Vastermark).

http://dx.doi.org/10.1016/j.jsb.2016.10.002
1047-8477/

2. Purpose

The rationale for this research is provided by considerations concerning the so called "Elevator Mechanism" (Vastermark and Saier, 2016). One of the four steps of the "Elevator Mechanism" involves a transition in which the substrate is captured (outward open to outward occluded transition). Recently, the outward occluded conformation of MalT of the GFL superfamily was solved, but the "substrate capturing step" could only be simulated using MD (McCoy et al., 2016). We have proposed that secondary structural elements can be mapped between the GFL superfamily (MalT, ChbC) and the ascorbate-galactitol (AG) superfamily (UlaA) (Vastermark and Saier, 2016) (Fig. 1, Table 1 in Vastermark et al. (2016) or Fig. S1 and Table S1). For this reason, we believe that the MD simulation of the substrate capturing step of GFL superfamily transporters can be partially "validated" by studying the alternative crystal forms of UlaA. Because the crystal contacts are the same between the alternative crystal forms, the differences seen cannot be attributed to contacts. Instead, we believe the alternative crystal forms can be found in the intermediates of the MD simulation (McCoy et al., 2016). The MD simulation suggests that it is the second half of the V-motifs (TMSs 2 and 7) that are involved in capturing the substrate, and that it is the mobile nature (presumably mediated by the critical glycines) that allows capture of the substrate (cf. outward open to occluded transition in UlaA, Fig. S2). In the alternative crystal forms of the outward open UlaA, the substrate is present, but in the transition to the outward occluded state, it is found that many salt bridges and substrate coordinating hydrogen bonds are rearranged. An interesting parallel can be drawn to the MFS (Radestock and Forrest, 2011) where a conserved movement of TMS11 releases the substrate on the inward side.

3. Background: PTS protein structures

The phosphoenolpyruvate (PEP):sugar phosphotransferase system (PTS) family of group translocators (TC #4.A; see TCDB, tcdb.org) is conceptually different from other major types of transport systems (e.g., primary active, secondary active or channel-based), in that the substrate is phosphorylated during transport (Vastermark and Saier, 2014). The transmembrane domains of PTS porters are traditionally designated Enzymes IIC (IICs), and can be grouped into several superfamilies. Members of different superfamilies are believed to be non-homologous (Saier et al., 2005). Other constituents of the PTS include the energy-coupling proteins, Enzyme I and HPr, and the phosphoryl transfer proteins, Enzymes IIA and IIB (IIA and IIB). High resolution structural information has been available for some time for two IIC proteins: the vitamin C transporter UlaA from *E. coli*, and the diacetylchitobiose transporter ChbC from *Bacillus cereus*.

4. Background: UlaA (TC# 4.A.7.1.1)

Bacteria, including intestinal *E. coli*, ferment vitamin C (L-ascorbic acid) as a carbon source, but mammals use it as a cytoplasmic reducing agent (Levine et al., 2011). Vitamin C is imported into *E. coli* by the transport system Ula (Utilization of ascorbic acid), which includes three proteins, IIA, IIB, and IIC^{Ula} (Luo et al., 2015; Zhang et al., 2003; Hvorup et al., 2003). In contrast, vitamin C uptake across the mammalian intestinal brush border is mediated by a sodium-dependent secondary carrier. The *E. coli* transporter has 10–25 times higher affinity (lower K_m) than intestinal secondary carriers (Jeckelmann et al., 2014; Boggavarapu et al., 2013), indicating that the bacteria can effectively compete with the intestinal mucosal cells.

The resolution of the X-ray structures of UlaA is 1.65 and 2.35 Å for the C2 and $P2_1$ space groups, respectively. The symmetry-related core domain coordinates vitamin C binding. Two major types of PTS group translocators include the "AG" type of which UlaA is a member (The PTS L-Ascorbate (L-Asc) Family (Zhang et al., 2003)), and the lactose family of the Glc-Fru-Lac ("GFL") superfamily (Nguyen et al., 2006), of which the chitobiose transporter ChbC is a member (McCoy et al., 2015; Cao et al., 2011). The AG and GFL superfamilies are not believed to be homologous and may have different evolutionary origins (Saier et al., 2014). In fact, at least four independently evolving EIICs are currently believed to exist within the PTS domain (Saier et al., 2005).

Since static light scattering experiments suggested that UlaA is a dimer in solution, the homodimeric partner in the C2 space group (PDB: 4RP9), indicated as C2A′, could be generated by a crystallographic two-fold axis (Luo et al., 2015). C2A and C2A′ are symmetry-related; therefore both of them have the same conformation. Only in the $P2_1$ space group (PDB: 4RP8) do the two different conformations, $P2_1$A and $P2_1$B, exist. From the structural superimposition, C2A is equivalent to (=) C2A′ = $P2_1$A ! = $P2_1$B (C2A, C2A′, and $P2_1$A are outward states, whereas $P2_1$B is the "occluded" state). In fact, we want to refute a suggestion (Luo et al., 2015) that the two protomers in the UlaA dimer function independently, as this suggestion disagrees with the cooperative model proposed for ChbC (Luo et al., 2015). The superimposition of C2A′ and $P2_1$B showed that while the structures are very similar, the core domain rotates 4.33° compared to the V motif, causing some atoms to move as much as 7 Å (Luo et al., 2015). The "rigid body" model is partly based on the fact that no conformational changes occur within the core domains, although rotational movement can be measured.

5. Methods

5.1. Protein expression and purification

We selected several homologs of UlaA from different prokaryotic genomes. Their cDNAs were cloned into pET15b and pET21b (Novagen). Please refer to published protocol in Luo et al. (2015) for the procedures used.

5.2. Preparation of proteoliposomes

Proteoliposomes were prepared following published protocols (Fang et al., 2007; Reig et al., 2007). An *E. coli* polar lipid extract (Avanti Polar Lipids) was prepared in CM buffer [chloroform: methanol, 3:1 (vol/vol)] to a final concentration of 50 mg/mL and then dried under a stream of nitrogen to remove the solvent and obtain thin layer dry lipids in a glass tube. The dried lipids were resuspended in inner reaction buffer (containing 25 mM Tris-HCl, pH 8.0, 150 mM NaCl) by vortexing for 20 min to yield a final lipid concentration of 20 mg/mL. After 10 cycles of quick freezing and thawing, the liposomes were extruded at least 21 times in an Avestin extruder through a 400-nm polycarbonate filter (Avanti) to obtain unilamellar vesicles of a homogeneous size. Protein concentration was determined using Bio-Rad reagents (Bradford Assay), and the liposomes were mixed with purified protein at a concentration of 50 μg/mg lipids. The ratio (by weight) of protein to lipid used to make proteoliposomes was 0.05. To destabilize the liposomes, β-D-octyl glucoside (OG) was added to a final concentration of 1.2%, followed by incubation at 4 °C for 2 h. DDM and OG were removed by incubating with 300 mg/mL Bio-Beads (Bio-Rad) overnight and then with 100 mg/mL Bio-Beads for 2 h. After five cycles of quick freezing and thawing, the proteoliposomes were extruded 21 times in the extruder through a 400-nm polycarbonate filter.

Finally, the proteoliposomes were ultracentrifuged at 100,000×g at 4 °C for 1 h, and the resulting pellet was resuspended in outer reaction buffer (containing 25 mM citrate, pH 5.0, 150 mM NaCl) to 100 mg/mL.

5.3. Transport assay

Each reaction system had a 3 μl volume of proteoliposomes and 97 μl outer reaction buffer (25 mM citrate, pH 5.0, 150 mM NaCl), 0.66 mM ^{14}C-ascorbate (5 μCi/ml). After incubating at 25 °C for 4 min, the proteoliposomes and free ^{14}C-ascorbate were vortexed and quickly placed onto a 0.45-μm filter (Sartorius) and washed in 2 mL ice-cold outer reaction buffer. Then the filter was placed into a 24-hole plate for liquid scintillation counting. All of the transport assays were repeated at least three times.

5.4. Δ-distance maps

Δ-distance maps were calculated as follows. The largest common set of Cα atoms was identified by the two conformational states of UlaA. Each state was represented as a matrix of all pairwise distance measurements. Bypassing previous convention (the "inward–outward" convention (Vastermark et al., 2015)), the matrix of the state (C2A) was subtracted from the ($P2_1A$) state.

The following parameters were used for ESCET normalization (Schneider, 2004). For 4RP8.A, D_{min} = 2.36 (resolution), N_{par} = 26,604 (number of parameters used in refinement, estimated), N_{obs} = 49,177 (number of reflections), Cpl = 96.1 (completeness), R_{free} = 0.239 (free R value; fit to data used in refinement), and R_{all} = 0.199 (R value, working and test set). For 4RP9, D_{min} = 1.65, N_{par} = 26,604, N_{obs} = 71,471, Cpl = 94.6, R_{free} = 0.174, and R_{all} = 0.136.

5.5. Normal Mode Analysis (NMA)

NOMAD-Ref (http://lorentz.immstr.pasteur.fr/nomad-Ref.php) was used with default parameters, calculating 36 modes of arbitrary collective motions of the C2A and $P2_1A$ states (the first six are trivial modes, translation and rotation), using an α-carbon representation. The average RMSD in output trajectories, the distance interaction weight parameter, and the cutoff to use for mode calculation were used with defaults (1, 5 and 10 Å, respectively) in the web server application.

6. Results

6.1. Identical crystal contacts suggest that alternative crystal forms of the outward open state might be substates of UlaA

The two open outward facing states (PDB: 4RP9 and 4RP8.A) show differences in the number of hydrogen bonds and salt bridges, as well as significant conformational differences (Figs. 3–6, and Tables 2 and 3 in Vastermark et al. (2016) or Figs. S3–6 and Tables S2–3). These differences could represent two stable, biologically relevant sub-conformations of the outward open state (C2A and $P2_1A$), or artifacts due to the conditions of crystallization, for example, the pH or salt concentration used during crystallization, or differences in the computational refinement steps.

The crystallization conditions could affect the orientation. Looking at BetP, for example, the presence and absence of substrate in the crystal bath (before forming crystals) or in a soak (after forming crystals) changes the conformation from substrate-free to substrate-bound (Perez et al., 2014). pH changes, or salt changes could alter whether sodium or protons are bound or not. It is also possible that there are sub-states formed under the same condition, especially if the crystals have formed in a different packing or symmetry group.

The unit cell dimensions of C2 and $P2_1$ lattices (C2, PDB ID 4RP9: 113.66, 85.81, 83.24, β = 127.98; $P2_1$, PDB ID 4RP8: 83.78, 85.56, 88.95, β = 96.73). It is noted that the unit cell volume of C2 is half the volume of $P2_1$. Actually the C2 diffraction data can be processed in a $P2_1$ lattice (with two protomers in asymmetric unit, a.u.). In this sense, the two $P2_1$ lattices have the same packing, but one with crystallographic 2-fold symmetry (e.g. C2) and the other lacking crystallographic symmetry (e.g. $P2_1$).

Crystallography (and single particle cryo EM) are the only techniques currently available for looking at detailed conformational changes in large transport proteins, but much can be influenced by the non-physiological environment imposed by the lattice. The differences between C2A and $P2_1A$ are small enough to be attributable to crystal packing differences. In contrast, the difference between outward open and occluded UlaA is large enough that it is unlikely that the reduction in energy due to crystal packing would be significant enough to induce such large conformational changes if the two states did not already represent states with comparable low energy in the native conformation.

For both C2A and $P2_1A$ forms, crystallization conditions were similar, where crystals were grown at 18° by the hanging drop vapor diffusion method, appearing after five days in the well buffer containing 0.1 M MES, pH 6.5, 0.1 M NaCl and 30% (v/v) PEG 400. To improve resolution, n-nonyl-ß-D-glucopyranoside (β-NG) was added at 0.4% to improve diffraction at 1.65 and 2.35 Å in the C2 and $P2_1$ space groups, respectively (Luo et al., 2015).

When dealing with crystallographic data, there is always a danger that observed structural differences could be artifacts of the crystal environment. This is particularly problematic for crystals of different space groups such as the two UlaA structures. To assess the potential for the differences between the C2A and $P2_1A$ forms having arisen from differences in crystal contacts, the crystal lattice for each protein state was generated and superimposed. Despite the different space groups, both structures form the same crystal lattice. All contacts with symmetry partners overlapped by at least 47% of the contacting residues, indicating a close equivalence between all crystal contacts (Fig. 1). Thus, the $P2_1$ lattice can be viewed as a slight deformation of the C2 lattice, eliminating the 2-fold crystallographic axis within the diad and presumably facilitating the conformational change of $P2_1B$ to the occluded state. The equivalence of the two lattices, and the similarity of the crystallization conditions, suggest that crystal contacts are unlikely to play a significant role in the observed structural differences. The term lattice refers to objects with perfect translational operators. The lattice is the grid of unit cells that together with the space group (the set of symmetric operators which relate molecules within the unit cell) form the crystal in a precise mathematical sense. A 2 × 2 × 2 chunk of the crystal lattice for the two structures have different shapes, different origins, and different numbers of asymmetric units per unit cell (although they have the same number of chains per cell). However, when they are superimposed, it can be seen that in the overlapping section, a UlaA monomer is located at equivalent positions in both lattices and has equivalent contacts with its neighbors. If the 2 × 2 × 2 grids were continued, we would see that all proteins overlap to within a few Angstroms. The overall arrangement of proteins (protein packing), or the crystal form (Xu et al., 2008), in each lattice is the same.

6.2. Homologous residues (Gly58 and 286) impact vitamin C transport

The homologous V motifs can be superimposed within the same state, revealing a 47° relative tilt and hinting that this segment may have been tilted through evolution (Fig. 2A). A structural

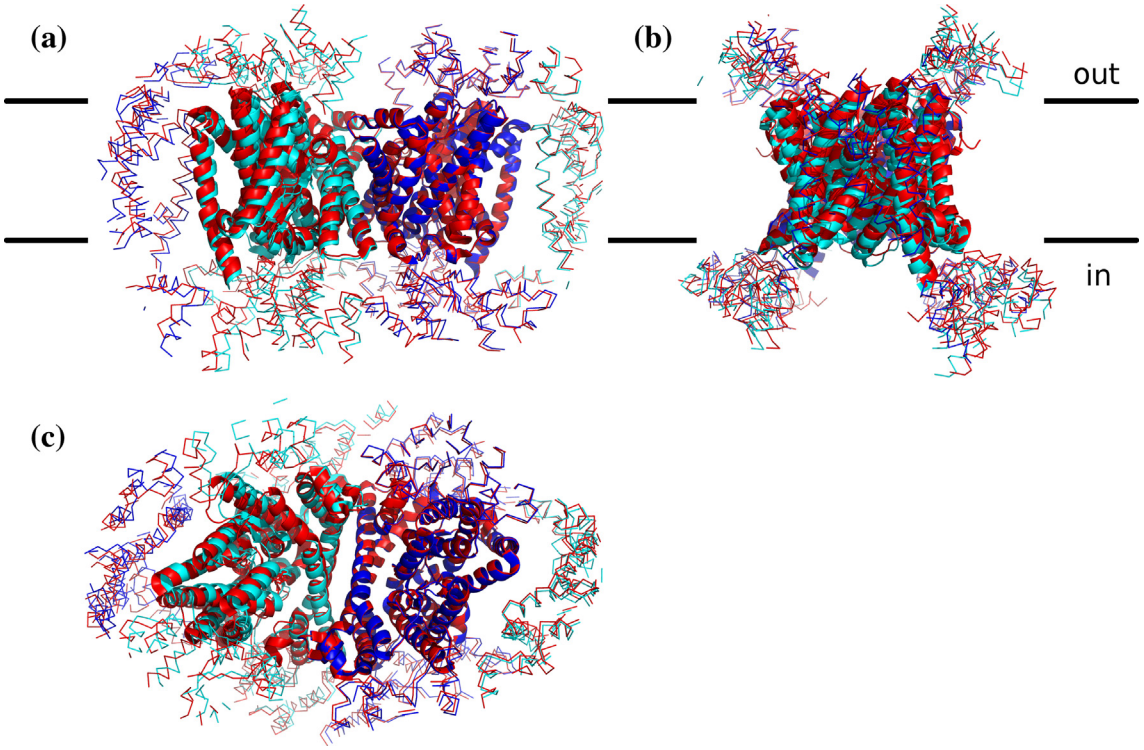

Fig. 1. Comparison of crystal contacts in both UlaA forms, using the same alignment but viewed from three different orientations (a, b, c). C2 data can be reprocessed in $P2_1$. One copy of the dimer is shown centrally from each structure, along with all contacting partners within 20 Å. The two outward open forms (red, C2A; blue, $P2_1A$) were superimposed. A deformation of the crystal lattice is visible due to the conformational change in $P2_1B$ (cyan), but all contacts are equivalent in the two structures (47–83% of contacting residues shared). Figure generated using PyMOL.

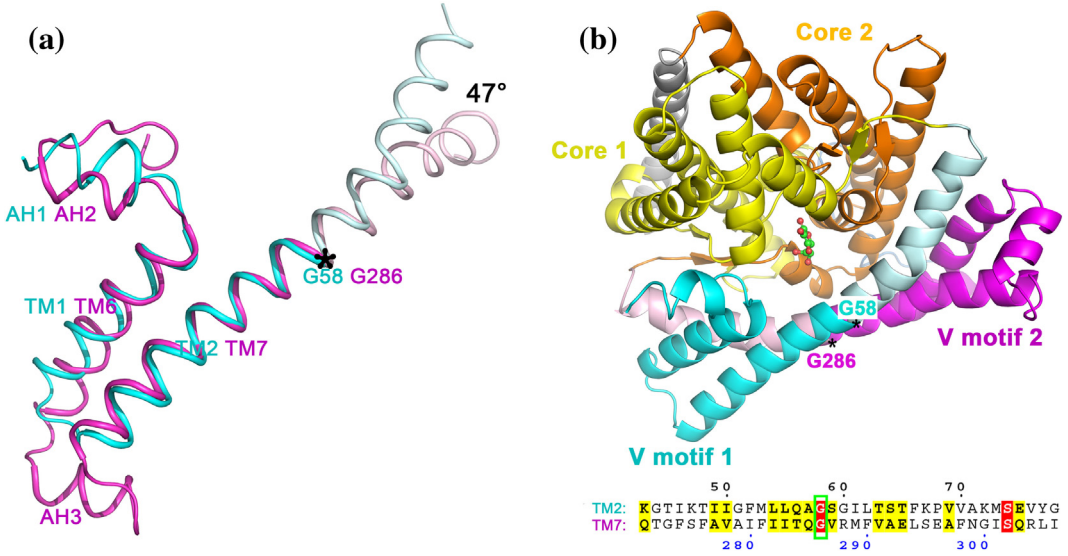

Fig. 2. Superimposition of "V motif 1" and "V motif 2" subdomains (a), and UlaA shown in cartoon representation, viewed from the extracellular space and tilted to reveal the binding site (b). Panel (a) is based on Fig. 3d in the original UlaA structure paper (Luo et al., 2015). C-termini of TMSs 2 and 7 have about 47° rotational movement, probably pivoted on the well conserved Gly58/Gly286. Note that this comparison (47°) is not observed between conformational states (e.g. the C2A ↔ $P2_1A$ to $P2_1B$ model); it is observed between V1 and V2 which share a TMS duplication origin. In panel (b), the C2 form corresponds to the outward-facing state, with "Core 2" oriented close to "V motif 2". The transport pivots Gly58 and Gly286 are indicated. The structure-based sequence alignment between TMSs 2 and 7 is displayed below the structure. The Gly58 and 286 residues align in the structural model (highlighted in red).

alignment shows that Gly58 and 286 are at homologous positions in their corresponding V domains (Fig. 2B). A time course for uptake of labeled vitamin C showed that uptake is severely impacted by replacing both functional glycines simultaneously by alanines, but that merely replacing Gly286 only reduced uptake by 50% compared to the combined knock-out effect (Fig. 3).

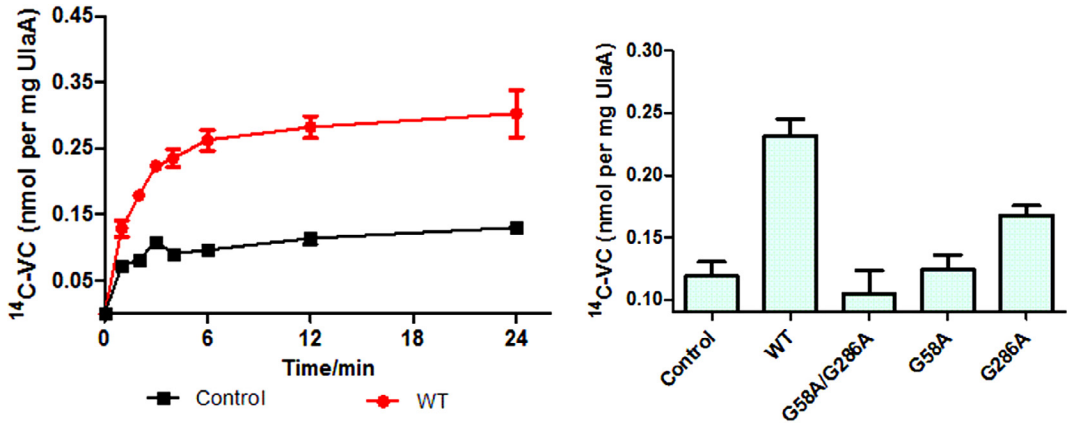

Fig. 3. Left, Time course of the uptake of ^{14}C-labelled vitamin C in proteoliposomes reconstituted with UlaA (red circles) or in control liposomes (black squares). Right, ^{14}C-vitamin C uptake assay identified the key pivotal residues Gly58 and Gly286 in the evolution of the vitamin C transporter. All of the transport assays were repeated at least three times. It was noticed that the control activity is higher than the G58A/G286A double mutant (measurement error).

6.3. TMS7 of MalT is comparatively short and contain conserved flanking glycines

It is not straightforward to align UlaA and MalT, but a GSAT alignment identified a conserved aligning motif close to TMS7 in both proteins (YXXXTG, Fig. 7 in Vastermark et al. (2016) or Fig. S7). The absence of sequence or structural evidence for a common ancestry provides the basis for suggesting these proteins are in different superfamilies in Transporter Classification Database (TCDB). However, secondary structural elements seem mappable (see supplementary file). A notable difference is that TMS7 is much shorter in MalT and appears to be flanked by rather than interspersed with glycine. G286 in UlaA has enough space around it to potentially accommodate a side-chain (Fig. 8 in Vastermark et al. (2016) or Fig. S8).

6.4. Differences between two outward open crystal forms of UlaA

The relative lack of internal movement between atoms contained within TMSs 3–5 and TMSs 8–10 of two crystal structures observed for UlaA agrees with the Luo et al. model of the outward open to outward occluded transition (Luo et al., 2015) (Fig. 4, symbol "A"). A blue line ("B"), probably representing a loop between TMSs 8 and 9, appears to have moved further away from the first core domain (denoted "core 1"; TMSs 3–5). In the transition between the C2A and the P2$_1$A crystal forms, the distance between V motif 1 and core 1 has increased. This is represented by the uniformly blue region of the plot, showing distance changes between TMSs 1–2 and 3–5 (Fig. 4; symbol "C"). The area of the plot showing distance remodeling between TMS6 of V motif 2 and TMSs 8–10 is red (suggesting decreased distance; Fig. 4; area "D"). TMS7, on the other hand, shows decreasing distance from TMS8, but increasing distance from TMSs 9–10 (area "E"). Considering the distance change within the V motifs, TMS1 appears to have separated from TMS2 in the transition to the more inward-facing state (area "F"). On the other hand, TMSs 6 and 7 have approached each other in the transition to the more inward-facing state (area "G"). It appears that the loops on the sides of TMS6 have approached both V motif 1 and the first core domain (area "H"), while TMS7 has clearly separated from both of these motifs ("H"). TMS1 has come closer to TMSs 8–10 whereas TMS2 appears to have moved away from TMSs 8–10 (symbol "I"; Fig. 4).

6.5. Normal mode simulation of outward open alternative states

Intrinsic conformational flexibility of outward open states of UlaA (PDB: 4RP9, 4RP8.A) agree with some flexible areas discovered by comparing the alternative crystal forms using distance maps. Loops flanking TMSs 2 and 7 (of V1 and V2) that had previously been identified in the distance map comparisons of the alternative crystal forms, C2A and P2$_1$A, were confirmed as being intrinsically flexible. The matrix of covariant motions for each mode are directly comparable to the distance map representing the difference between the outward open conformations of UlaA (after scaling), helping us to disentangle the total difference between the outward open crystal forms and components of that movement. The NMA of the C2A and P2$_1$A crystal forms of UlaA revealed that the intrinsic flexibility conforms to the conformational switching between the alternative crystal forms. Some aspects of the mechanism of action (flexibility around the V motif) are consistent with both the crystal structures and the NMA.

6.6. Interpretation of MalT MD simulation of substrate catching

The 2nd V (approx. 240–280 residues, TMS 6–7 and beta 5–6) moved between 5 and 10 ns in the "Rep 1" experiment (triplicate 1, Fig. 9A in Vastermark et al. (2016) or Fig. S9A). The 2nd V moved between 5 and 10 ns (and between 20 and 25 ns) in the "Rep 3" experiment (triplicate 3, Fig. 11 in Vastermark et al. (2016), or Fig. S11, panels A and D). This observation is consistent with an oscillation between two substates of outward open, and consistent with movement of the substrate catching TMS. We can infer that for triplicate 3, comparing time point 5 and 25 (or 10 and 20 ns) would give no oscillatory signal. For triplicate 3, comparing time point 25 and 10 (or 5 and 15) would give "signal" (2nd V moved).

7. Conclusion

We present an unusual case in this paper, of greater theoretical than practical importance, comparing alternative crystal forms of the outward open state of UlaA as a new source of molecular flexibility data. One of the main differences between NMA data and temperature factor is that the latter gives an aggregate for a particular position, while the raw NMA data show collective movements. Alternative crystal data provide a "hybrid" between the two, in the sense that it is limited by crystal contacts, but shows collective movement between two sub-states (Fig. 5). The strength of the

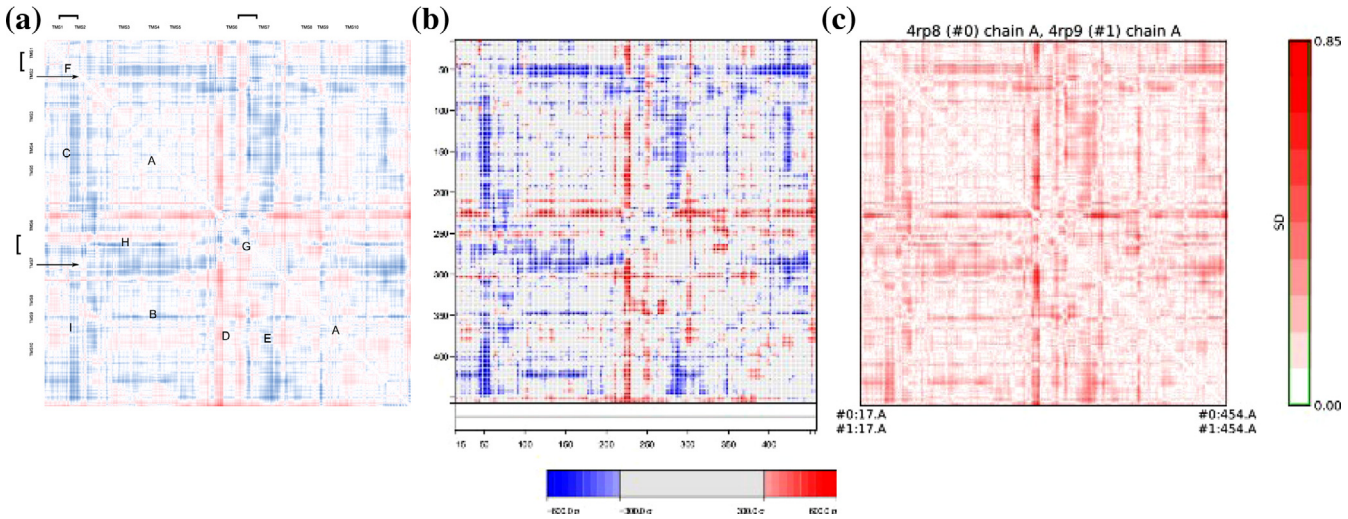

Fig. 4. Δ-distance maps representing the difference between the outward open C2A and $P2_1A$ crystal forms of UlaA. (A) Bypassing the "inward–outward" convention established earlier, we determined the PDB: 4RP8.A-4RP9 distance map. As above, blue indicates a positive number, red, a negative number. Hence, blue coloring means the distance in the $P2_1A$ state of UlaA (PDB: 4RP8.A) is greater than in the C2A conformation of UlaA (PDB: 4RP9), or that the corresponding atomic distance increased. For example, the distance between the N-terminal ends of TMS2 and TMS4 increased, including the distance between Ile42 (atom# CD1) and Gln140 (atom# OE1), which increased from 33.4 Å (4RP9) to 34.0 Å (4RP8) (hence colored blue). Conversely, the distance between mid-TMS6 and a loop between TMSs 8–9 (including atoms #CB of Ile242 CB & CD2 of Leu352) decreased from >27.4 Å (4RP9) to <27.4 Å (4RP8) (hence colored red). The color scale used goes from approximately −1.5 to +1.5 Å, but most cells have absolute values that are smaller than ±0.5 Å. The two horizontal arrows indicate the positions of the pivotal residues Gly58 and Gly286. Gly58 appears to be associated with a 7 residues-wide stationary region, possibly associated with the need to uncouple TMS2 movement from mid TMS2 residues interacting with the substrate. (B) ESCET 0.7 was used to normalize the diagram. What appears red and blue in the normalized diagram is >300 σ more extreme than the background, indicating that the differences are greater than the resolution limit of both structures. (C) RR distance maps in Chimera 1.10 were used to determine that the "red cross" reached 0.85 S.D. but that the two "blue crosses" were closer to 0.5 S.D.

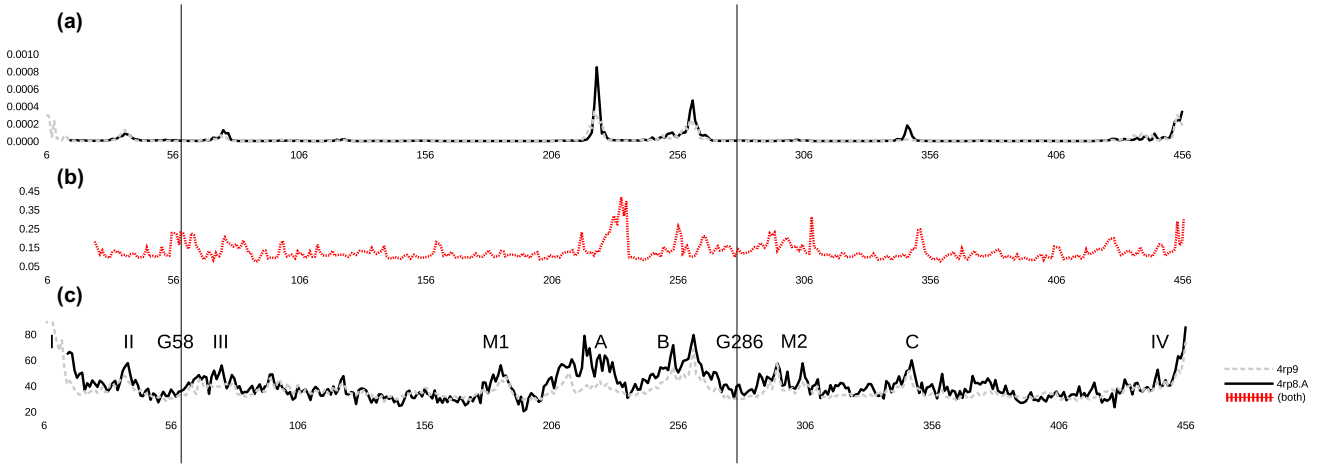

Fig. 5. Comparison of alternative crystal forms of UlaA using a) NMA, b) Δ-distance map, and c) temperature factor. NOMAD-Ref was used to calculate non-trivial modes. The Δ-distance comparison of the alternative crystal states represents an "intermediate" between NMA and temperature factor, because these data are constrained by the crystal lattice, yet represent idealized combined motions. Some flexibility (M1 and M2) are missing in the NMA graph. Residues 6–15 are missing in one of the substates (PDB: 4RP8.A), removing a crystal contact and giving the (dashed, grey) curve an elevated mobility in the N-terminal region. While $P2_1A$ state of UlaA (PDB: 4RP8.A) generally displays higher peaks in the merged NMA graph, the C2A conformation of UlaA (PDB: 4RP9) has a higher unrestrained mobility in the N-terminus. However, if crystal contacts are taken into account, the peaks I and II of the $P2_1A$ state of UlaA (PDB: 4RP8.A) line are decimated. The residues of functional interest, G58 and G286 are part of beginning of peak III and M2, respectively. The positions of G58 and G286 are indicated by two vertical lines, one for each residue, across three plots. Notice that "missing" area M1 cannot be seen in the alternative crystal comparison plot (b), while "M2" can be seen. The crystal contacts are identical between (C2A) and ($P2_1A$), with instability peaks generally located between contacts. No NMA movement was found in crystal contact regions. It might have biological significance, that only the M2 area shows up as instability in the crystal comparison, meaning that conformation change in M2 area is involved in switching between (C2A) and ($P2_1A$) sub-states.

alt crystal data might be that it represents two real low energy collective states that the protein prefers, in the crystal hindering environment.

8. Discussion

The role of the PTS regulatory functions in addition to transport might provide insight into the undifferentiated evolution between transporters and receptors, including receptors that bind substrates without signaling (Västermark et al., 2013). The concept of comparing NMA and B-factor data is not new, it was first considered by Hinsen (2008), and he concluded that the differences are attributable to the crystal contacts. Of course, NMA is most effective to simulate large scale movements, not the small differences observed between alternative crystal forms. There is even an approach known as "crystal simulation" where MD simulations

are performed in the crystal environment. NMA is a very attractive method, although it has lost most of its popularity; it is a method that can be used in a resource poor environment. Proteins have even been rationally designed to create CCFS (crystal contact free space) to study how crystal contacts affect motion (Matsuoka et al., 2016). A standardized method for comparing beta factor and NMA plots is under development, where vectors and mode frequencies are added up to create a single beta factor-like curve. A similar baseline is established and a transform such as discrete cosine transform-II is used to make the curves easy to compare.

Competing interests statement

The authors declare that they have no competing interests.

Author contributions

AV, AD wrote the paper. JWa, XL contributed experimental data. JWe carried our Normal Mode simulations. AV, MHS conceived of the study, and participated in its design and coordination.

Acknowledgements

The work was supported by NIH grants GM077402 and GM094610 (to M.S.) and by funds from the Ministry of Science and Technology of China (grant nos. 2011CB911102 and 2015CB910104) and the National Natural Science Foundation of China (31321062) to J.W. We are grateful for valuable advice and intellectual contributions (lattice analysis) by Dr. Spencer Bliven, Bioinformatics and Systems Biology, University of California at San Diego, La Jolla, CA 92093-0116, USA & National Center for Biotechnology Information, National Library of Medicine, National Institutes of Health, Bethesda, MD 20894, USA. We thank Dr. Wonpil Im, Kansas University, for providing the original MalT simulation data.

Appendix A. Supplementary data

Supplementary data associated with this article can be found, in the online version, at http://dx.doi.org/10.1016/j.jsb.2016.10.002.

References

Boggavarapu, R., Jeckelmann, J.M., Harder, D., Schneider, P., Ucurum, Z., Hediger, M., Fotiadis, D., 2013. Expression, purification and low-resolution structure of human vitamin C transporter SVCT1 (SLC23A1). PLoS One 8 (10), e76427.

Cao, Y., Jin, X., Levin, E.J., Huang, H., Zong, Y., Quick, M., Weng, J., Pan, Y., Love, J., Punta, M., 2011. Crystal structure of a phosphorylation-coupled saccharide transporter. Nature 473 (7345), 50–54.

Fang, Y., Kolmakova-Partensky, L., Miller, C., 2007. A bacterial arginine-agmatine exchange transporter involved in extreme acid resistance. J. Biol. Chem. 282 (1), 176–182.

Hinsen, K., 2008. Structural flexibility in proteins: impact of the crystal environment. Bioinformatics 24 (4), 521–528.

Hvorup, R., Chang, A.B., Saier Jr., M.H., 2003. Bioinformatic analyses of the bacterial L-ascorbate phosphotransferase system permease family. J. Mol. Microbiol. Biotechnol. 6 (3–4), 191–205.

Jeckelmann, J.M., Harder, D., Ucurum, Z., Fotiadis, D., 2014. 2D and 3D crystallization of a bacterial homologue of human vitamin C membrane transport proteins. J. Struct. Biol. 188 (1), 87–91.

Levine, M., Padayatty, S.J., Espey, M.G., 2011. Vitamin C: a concentration-function approach yields pharmacology and therapeutic discoveries. Adv. Nutr. 2 (2), 78–88.

Luo, P., Yu, X., Wang, W., Fan, S., Li, X., Wang, J., 2015. Crystal structure of a phosphorylation-coupled vitamin C transporter. Nat. Struct. Mol. Biol. 22 (3), 238–241.

Matsuoka, R., Shimada, A., Komuro, Y., Sugita, Y., Kohda, D., 2016. Rational design of crystal contact-free space in protein crystals for analyzing spatial distribution of motions within protein molecules. Protein Sci. 25 (3), 754–768.

McCoy, J.G., Levin, E.J., Zhou, M., 2015. Structural insight into the PTS sugar transporter EIIC. Biochim. Biophys. Acta 1850 (3), 577–585.

McCoy, J.G., Ren, Z., Stanevich, V., Lee, J., Mitra, S., Levin, E.J., Poget, S., Quick, M., Im, W., Zhou, M., 2016. The structure of a sugar transporter of the glucose EIIC superfamily provides insight into the elevator mechanism of membrane transport. Structure 24 (6), 956–964.

Nguyen, T.X., Yen, M.R., Barabote, R.D., Saier Jr., M.H., 2006. Topological predictions for integral membrane permeases of the phosphoenolpyruvate: sugar phosphotransferase system. J. Mol. Microbiol. Biotechnol. 11 (6), 345–360.

Perez, C., Faust, B., Mehdipour, A.R., Francesconi, K.A., Forrest, L.R., Ziegler, C., 2014. Substrate-bound outward-open state of the betaine transporter BetP provides insights into Na+ coupling. Nat. Commun. 5, 4231.

Radestock, S., Forrest, L.R., 2011. The alternating-access mechanism of MFS transporters arises from inverted-topology repeats. J. Mol. Biol. 407 (5), 698–715.

Reig, N., del Rio, C., Casagrande, F., Ratera, M., Gelpi, J.L., Torrents, D., Henderson, P.J., Xie, H., Baldwin, S.A., Zorzano, A., 2007. Functional and structural characterization of the first prokaryotic member of the L-amino acid transporter (LAT) family: a model for APC transporters. J. Biol. Chem. 282 (18), 13270–13281.

Saier, M.H., Hvorup, R.N., Barabote, R.D., 2005. Evolution of the bacterial phosphotransferase system: from carriers and enzymes to group translocators. Biochem. Soc. Trans. 33 (Pt. 1), 220–224.

Saier Jr., M.H., Reddy, V.S., Tamang, D.G., Vastermark, A., 2014. The transporter classification database. Nucleic Acids Res. 42 (Database issue), D251–D258.

Schneider, T.R., 2004. Domain identification by iterative analysis of error-scaled difference distance matrices. Acta Crystallogr. D Biol. Crystallogr. 60 (Pt 12 Pt 1), 2269–2275.

Västermark, Å., Saier Jr., M.H., 2014. Evolutionary relationship between 5+5 and 7+7 inverted repeat folds within the amino acid-polyamine-organocation superfamily. Proteins 82 (2), 336–346.

Vastermark, A., Saier Jr., M.H., 2014. The involvement of transport proteins in transcriptional and metabolic regulation. Curr. Opin. Microbiol. 18, 8–15.

Vastermark, A., Saier Jr., M.H., 2016. Time to stop holding the elevator: a new piece of the transport protein mechanism puzzle. Structure 24 (6), 845–846.

Västermark, Å., Rask-Andersen, M., Sawant, R.S., Reiter, J.L., Schiöth, H.B., Williams, M.J., 2013. Insulin receptor-like ectodomain genes and splice variants are found in both arthropods and human brain cDNA. J. Syst. Evol. 51 (6), 664–670.

Vastermark, A., Driker, A., Li, J., Saier Jr., M.H., 2015. Conserved movement of TMS11 between occluded conformations of LacY and XylE of the major facilitator superfamily suggests a similar hinge-like mechanism. Proteins 83 (4), 735–745.

Vastermark, A., Driker, A., Weng, J., Li, X., Wang, J., Saier, M.H., 2016. Data Generated Comparing Alternative Crystal Forms of UlaA. Data in Brief Submitted.

Xu, Q., Canutescu, A.A., Wang, G., Shapovalov, M., Obradovic, Z., Dunbrack Jr., R.L., 2008. Statistical analysis of interface similarity in crystals of homologous proteins. J. Mol. Biol. 381 (2), 487–507.

Zhang, Z., Aboulwafa, M., Smith, M.H., Saier Jr., M.H., 2003. The ascorbate transporter of *Escherichia coli*. J. Bacteriol. 185 (7), 2243–2250.